CHEMISTRY OF MATERIALS
Cite This: Chem. Mater. 2019, 31, 919−926
Article
pubs.acs.org/cm

A Benzobis(thiazole)-Based Copolymer for Highly Efficient Non-Fullerene Polymer Solar Cells

Shuguang Wen,*[†] Yi Li,[‡] Thomas Rath,[§] Yonghai Li,[†] Yao Wu,[†] Xichang Bao,[†] Liangliang Han,[†] Heike Ehmann,[∥] Gregor Trimmel,*[§] Yong Zhang,[‡] and Renqiang Yang*[†]

[†]CAS Key Laboratory of Bio-based Materials, Qingdao Institute of Bioenergy and Bioprocess Technology, Chinese Academy of Sciences, Qingdao 266101, China

[‡]Laboratory of Nanophotonic Functional Materials and Devices, Institute of Optoelectronic Materials and Technology, South China Normal University, Guangzhou 510631, China

[§]Institute for Chemistry and Technology of Materials (ICTM), NAWI Graz, Graz University of Technology, Stremayrgasse 9, 8010 Graz, Austria

[∥]Anton Paar GmbH, Anton-Paar-Straße 20, 8054 Graz, Austria

Supporting Information

ABSTRACT: In recent years, non-fullerene polymer solar cells have attracted much attention due to their great potential for achieving high power conversion efficiencies, and in addition to the already existing donor polymers, varieties of excellent acceptors have been developed. To further improve the performance, the main challenge is now to identify perfect donor−acceptor pairs with suitable electronic properties and complementary optical absorption. In this article, we have investigated a donor−acceptor alternating copolymer poly-[(4,8-bis(5-(2-ethylhexyl)thiophen-2-yl)benzo[1,2-*b*:4,5-*b*′]-dithiophene)-2,6-diyl-*alt*-(2,6-bis(5-bromo-4-(2-butyloctyl) thiophen-2-yl)benzo[1,2-*d*:4,5-*d*′]bis(thiazole))] with benzo-[1,2-*d*:4,5-*d*′]bis(thiazole) (BBT) as the accepting unit and benzo[1,2-*b*:4,5-*b*′]dithiophene as the donor unit. The polymer shows a wide band gap of 2.1 eV with absorption peaks at 515 and 554 nm, matching well with the strongest region of the solar radiation spectrum. A blend of this polymer with the narrow-bandgap acceptor ITIC-F, (3,9-bis(2-methylene-(3-(1,1-dicyanomethylene)-6-fluoro-indanone))-5,5,11,11-tetrakis(4-hexyl-phenyl)-dithieno[2,3-*d*:2′,3′-*d*′]-*s*-indaceno[1,2-*b*:5,6-*b*′]dithiophene)(mixture with 7-fluoro-indanone isomer), as the active layer in combination with a solvent vapor annealing process led to solar cells exhibiting a high efficiency of 13.3% with an open-circuit voltage of 0.91 V, a short current density of 20.9 mA cm^{-2}, and a fill factor of 0.70. The solvent vapor annealing method led to an improvement of the molecular packing, exciton dissociation, and charge transport, thus enhancing the power conversion efficiency. It is noteworthy that external quantum efficiency spectra show excellent photoresponse, especially in the wavelength range from 430 to 570 nm, demonstrating that this donor−acceptor combination efficiently absorbs in the wavelength range where the solar radiation spectrum has its maximum. The results indicate that polymers based on BBT are very promising candidates for high-performance non-fullerene polymer solar cells.

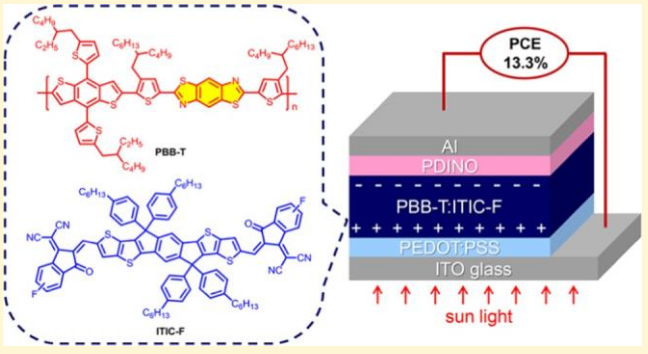

INTRODUCTION

In recent years, polymer solar cells (PSCs) have attracted extensive attention due to their flexibility, light weight, and the prospects of fast and cost-efficient large area production, also allowing nonstandard applications of photovoltaics such as integration in wearable electronic devices.[1−5] The active layer of PSCs is usually composed of donor and acceptor materials with a bulk heterojunction structure, which is proved to be an effective device structure to facilitate charge separation and transport.[6,7] Traditional fullerene-based acceptor materials have some inherent drawbacks, such as weak optical absorption, difficulty in modification, and instability, which might hinder further development of PSCs.[8] Non-fullerene acceptors, especially the acceptor−donor−acceptor (A−D−A)-type small molecular acceptors (SMAs), have made great progress during the last 3 years.[9−17] Compared with fullerene acceptors, the major advantages of SMAs are that the molecular structure can be easily modified and the energy levels can also be modulated as needed, which enable them to exhibit a much better optical absorption ability and, especially, the absorption range to be extended to over 900 nm. Therefore, nowadays very efficient narrow-bandgap acceptors

Received: October 8, 2018
Revised: January 14, 2019
Published: January 16, 2019

DOI: 10.1021/acs.chemmater.8b04265
Chem. Mater. 2019, 31, 919−926

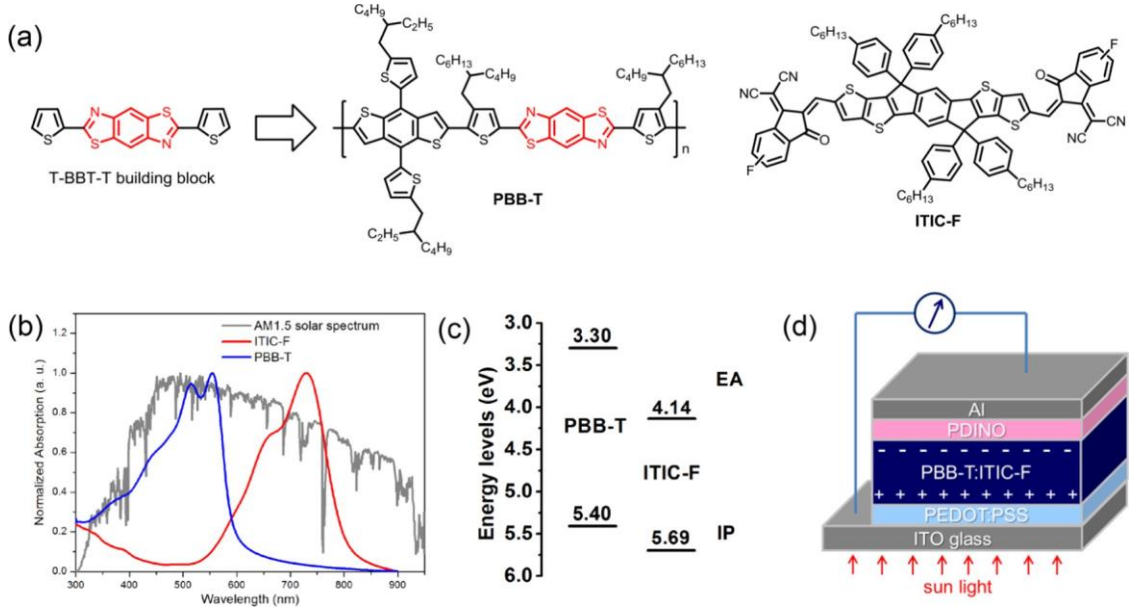

Figure 1. (a) Chemical structures of PBB-T and ITIC-F, (b) solar radiation spectrum and UV−vis absorption spectra of PBB-T and ITIC-F in thin films, (c) energy level diagram of PBB-T and ITIC-F, and (d) device architecture.

are available.[18−23] However, today one of the major challenges in this field is to find the perfect partners from the vast number of structures known in the literature. This is even more complicated because many of them are only basically characterized and thus their full photovoltaic potential is unexplored. Regarding narrow-bandgap acceptors, finding donor materials with complementary optical absorption is an effective strategy to utilize the solar energy in an optimum manner, and consequently some wide-bandgap polymers have been studied as donor materials.[24−29] Among them, the polymers based on fluorobenzotriazole (FTAZ) and benzo[1,2-*c*:4,5-*c*′]dithiophene-4,8-dione (BDD) are of high importance.[30,31] The corresponding copolymers with benzo[1,2-*b*:4,5-*b*′]dithiophene (BDT) exhibit their maximum absorption above 600 nm. However, the strongest solar radiation region is at a wavelength around 500 nm and the intensity is gradually reduced in the longer wavelength region. Thus, polymers based on FTAZ and BDD do not utilize the solar radiation spectrum in an optimum manner, and consequently, the photoresponse of solar cells with these polymers is limited in the region around 500 nm.[27,32]

Benzo[1,2-*d*:4,5-*d*′]bis(thiazole) (BBT) is a weak electron-withdrawing building block compared with FTAZ and BDD, which can be suitable for the construction of relatively large-bandgap organic semiconductors,[33,3433,34] and the absorption peaks of some BBT-based polymers are generally at wavelengths between 500 and 560 nm, which is well matching with the maximum region of the solar radiation spectrum.[35−37] Furthermore, BBT-based polymers show good mobility and durability in organic field-effect transistors[35,38] and have also been investigated in solar cells.[39] Based on this, it can be expected that the combination of BBT-based polymers and non-fullerene acceptors will lead to highly efficient solar cells. In this work, we synthesized the copolymer poly[(4,8-bis(5-(2-ethylhexyl)thiophen-2-yl)benzo[1,2-*b*:4,5-*b*′]dithiophene)-2,6-diyl-*alt*-(2,6-bis(5-bromo-4-(2-butyloctyl) thiophen-2-yl)-benzo[1,2-*d*:4,5-*d*′]bis(thiazole))] (PBB-T) with the alternating structure BDT-*alt*-T-BBT-T (for the chemical structure, see Figure 1). The BDT-*alt*-T-BBT-T structural motif was introduced by Bhuwalka et al. in short oligomers showing low power conversion efficiencies (1.62%) in combination with PCBM.[37] By changing the side chains and optimizing the polymerization conditions, we were able to synthesize the polymer PBB-T with a high molecular weight for the first time. The absorption peaks of PBB-T are located at 515 and 554 nm with a wide optical band gap of 2.10 eV. Among the efficient narrow-bandgap absorbers, ITIC-F was selected because it has already shown high efficiencies in other donor−acceptor systems[36] and has an almost perfect complementary absorption profile. With this combination, solar cells with a high efficiency of 13.3% were achieved with an open-circuit voltage (V_{OC}) of 0.91 V, a short current density (J_{SC}) of 20.9 mA cm^{-2}, and a fill factor (FF) of 0.70. These results indicate that PBB-T is a promising wide-bandgap polymer donor material for non-fullerene PSCs.

RESULTS AND DISCUSSION

Synthesis. The synthetic procedure of the polymer PBB-T is shown in Figure S1. The T-BBT-T unit (monomer 2) is obtained by the reaction of 4-(2-butyloctyl)thiophene-2-aldehyde and 2,5-diaminobenzene-1,4-dithiol in good yield and subsequent bromination.[37] 4-(2-Butyloctyl) side chains were employed on the thiophene units to guarantee the solubility of the polymer. Monomer 2 is then reacted with the corresponding BDT unit (monomer 3) by a Pd-catalyzed Stille coupling reaction to produce the polymer PBB-T. The molecular weight of the polymer was measured by gel permeation chromatography (GPC) using 1,2,4-trichlorobenzene (TCB) as the solvent and polystyrene as the standard at 150 °C. The number-average molecular weight (M_n) of PBB-T shows a high value of 107 kDa with a polydispersity index (PDI) of 2.52. The polymer is readily soluble at room temperature in common organic solvents such as chloroform, toluene, or chlorobenzene, but shows limited solubility in tetrahydrofuran. The thermogravimetric analysis (Figure S2) reveals a high thermal stability of PBB-T with a decomposition

DOI: 10.1021/acs.chemmater.8b04265
Chem. Mater. 2019, 31, 919−926

temperature (5% weight loss) of 352 °C. Differential scanning calorimetry was performed and no obvious glass transition (T_g) was observed even when heated up to 260 °C (Figure S3). The lack of observable T_g could be mainly attributed to the rigid polyaromatic structure.[40]

Photophysical and Electrochemical Properties. Figure 1b shows the absorption spectra of PBB-T and ITIC-F in films. The polymer PBB-T exhibits two absorption peaks at 515 and 554 nm and shows a wide optical band gap (E_g^{opt}) of 2.10 eV as calculated from the absorption onset at 591 nm, which is in the range of the strongest region of the solar radiation spectrum and is wider than for polymers such as P3HT,[23] PBDB-T,[32] or J61.[24] Compared with the absorption in films, PBB-T exhibits a slight blueshift (~2 nm) of the absorption maximum in solution (Figure S4). An obvious shoulder peak is also observed in solution. With increasing temperature, the intermolecular interaction is broken and the shoulder peak diminishes gradually along with a blueshift of the absorption peak, indicating a strong intermolecular stacking interaction for the polymer. A high absorption coefficient of 9.0×10^4 cm^{-1} was determined for the polymer film (Figure S12). The solid film of ITIC-F displays a strong absorption in the range between 600 and 800 nm with an optical band gap of 1.55 eV. The optical and electronic properties of the materials are summarized in Table 1. It is obvious that donor and acceptor materials exhibit complementary optical absorption, which is beneficial for optimum sunlight harvesting.

Table 1. Electronic and Optical Properties of PBB-T and ITIC-F

materials	λ_{max} (nm) as film	λ_{edge} (nm)	E_g^{opt}[a] (eV)	IP[b] (eV)	EA[b] (eV)	EA^{opt}[c] (eV)
PBB-T	515, 554	591	2.10	5.40	3.17	3.30
ITIC-F	730	798	1.55	5.69	3.93	4.14

[a]Calculated from the absorption spectrum edge of films using the equation $E_g^{opt} = 1240/\lambda_{edge}$. [b]Measured by CV. [c]Estimated using the equation $EA^{opt} = IP - E_g^{opt}$, where the exciton binding energy is neglected.

The ionization energies of PBB-T and ITIC-F were measured by electrochemical cyclic voltammetry (CV) with ferrocene (4.8 eV) as the standard reference (Figure S5). The ionization potential (IP) and electron affinity (EA) of PBB-T are estimated to be 5.40 and 3.17 eV from the onset of the oxidation and reduction potential. Accordingly, the IP and EA of ITIC-F are 5.69 and 3.93 eV, respectively. The IP and EA offsets of PBB-T:ITIC-F are 0.29 and 0.76 eV, respectively. It is generally accepted that an energy level offset of 0.3 eV could provide enough driving force for efficient exciton dissociation, but it seems not necessary for non-fullerene PSCs.[42] To confirm the exciton dissociation in the blend, photoluminescence (PL) spectra of a pristine PBB-T and a PBB-T:ITIC-F (ratio 1:1.2) blend film were measured, as shown in Figure S6. It is observed that the blend film shows a quenching efficiency of 98.5% at an excitation wavelength of 500 nm, indicating an effective electron transfer from PBB-T to ITIC-F. Excited at 600 nm, the blend film shows a quenching efficiency of 94.7% of the PL spectrum of ITIC-F, which indicates that the holes can also be transferred efficiently from the acceptor to the donor material.

Photovoltaic Properties. PSC devices were fabricated in the configuration glass/ITO (indium tin oxide)/PEDOT:PSS (poly(3,4-ethylenedioxythiophene):poly(styrene-sulfonate))/PBB-T:ITIC-F/PDINO (perylene diimide functionalized with amino *N*-oxide[43])/Al (see also Figure 1d). The photovoltaic performance of the devices was optimized and the detailed results are shown in Table S1 in the Supporting Information. Figure 2a shows current density−voltage ($J-V$) curves of typical devices and the photovoltaic parameters are summarized in Table 2. The optimized weight ratio of PBB-T:ITIC-F is found to be 1:1.2, which showed a high PCE of 11.3%, with a V_{OC} of 0.92 V, a J_{SC} of 19.7 mA cm^{-2}, and an FF of 0.62 for the device with an as-cast blend film. Solvent additives such as 1,8-diiodooctane and chloronaphthalene have not been beneficial for improving the device efficiency. After thermal annealing at 150 °C for 10 min, the PCE is improved to 12.8%, with a slightly higher V_{OC} of 0.93 V, a higher J_{SC} of 20.5 mA cm^{-2}, and an FF of 0.67. To further improve the efficiency, solvent vapor annealing (SVA) is performed in a chlorobenzene atmosphere (Table S2). For this, after spin coating the active layer, the devices were placed in an atmosphere of chlorobenzene at 150 °C for 10 min (a detailed description of the SVA procedure is given in the Supporting Information). After that, the devices were completed by adding a PDINO layer and the back contact. An excellent PCE of 13.3% is achieved with a V_{OC} of 0.91 V, a J_{SC} of 20.9 mA cm^{-2}, and an FF of 0.70. This result indicates that the SVA treatment with thermal annealing is an effective approach for improving the device performance. It is also noteworthy that all of the devices generally exhibit high J_{SC} values of about 20 mA cm^{-2}, whereas mainly the FF was improved by the optimization of the annealing conditions. The statistics of the PCEs of 20 devices are summarized in Figure S11. It shows a narrow distribution of PCEs around 13.2%, indicating the good reproducibility and excellent performance of the PSCs. We have also synthesized another batch of this polymer by a $Pd(PPh_3)_4$-catalyzed reaction. The polymer shows a lower molecular weight of 71.4 K with a PDI of 2.63. With this batch, a lower power conversion efficiency of 11.4% was obtained with a V_{OC} of 0.91 V, a J_{SC} of 19.1 mA cm^{-2}, and an FF of 0.66 with SVA treatment, which demonstrates the importance of molecular weight in the performance of solar cells.

External quantum efficiency (EQE) spectra of the devices based on PBB-T:ITIC-F (1:1.2, w/w) are shown in Figure 2b. Both donor and acceptor materials contribute effectively to current generation. A high maximum EQE value of about 84% is obtained with a wide photoresponse from 300 to 800 nm. Importantly, the polymer donor exhibits high EQE values of over 80% in the wavelength range of 430−570 nm, which indicates the effective utilization of the strongest region of the solar radiation spectrum. This, together with the high EQE values in the absorption region of ITIC-F up to 800 nm, leads to such high J_{SC} values. Solvent vapor annealing slightly expands the photoresponse range, which is in accordance with the UV−vis absorption data (Figure S7) and is beneficial for a higher J_{SC}. The J_{SC} values integrated from the EQE spectra are in good agreement with those measured from $J-V$ tests within a 5% error.

To investigate the exciton dissociation and charge collection behavior of the PSC devices, the dependence of photocurrent density (J_{ph}) on the effective voltage (V_{eff}) was measured,[44] as shown in Figure 2c. J_{ph} is defined as $J_L - J_D$, where J_L and J_D are the current densities under illumination and in the dark, respectively. V_{eff} is defined as $V_0 - V_{bi}$, where V_0 is the voltage at which the current is zero and V_{bi} is the applied bias

DOI: 10.1021/acs.chemmater.8b04265
Chem. Mater. 2019, 31, 919−926

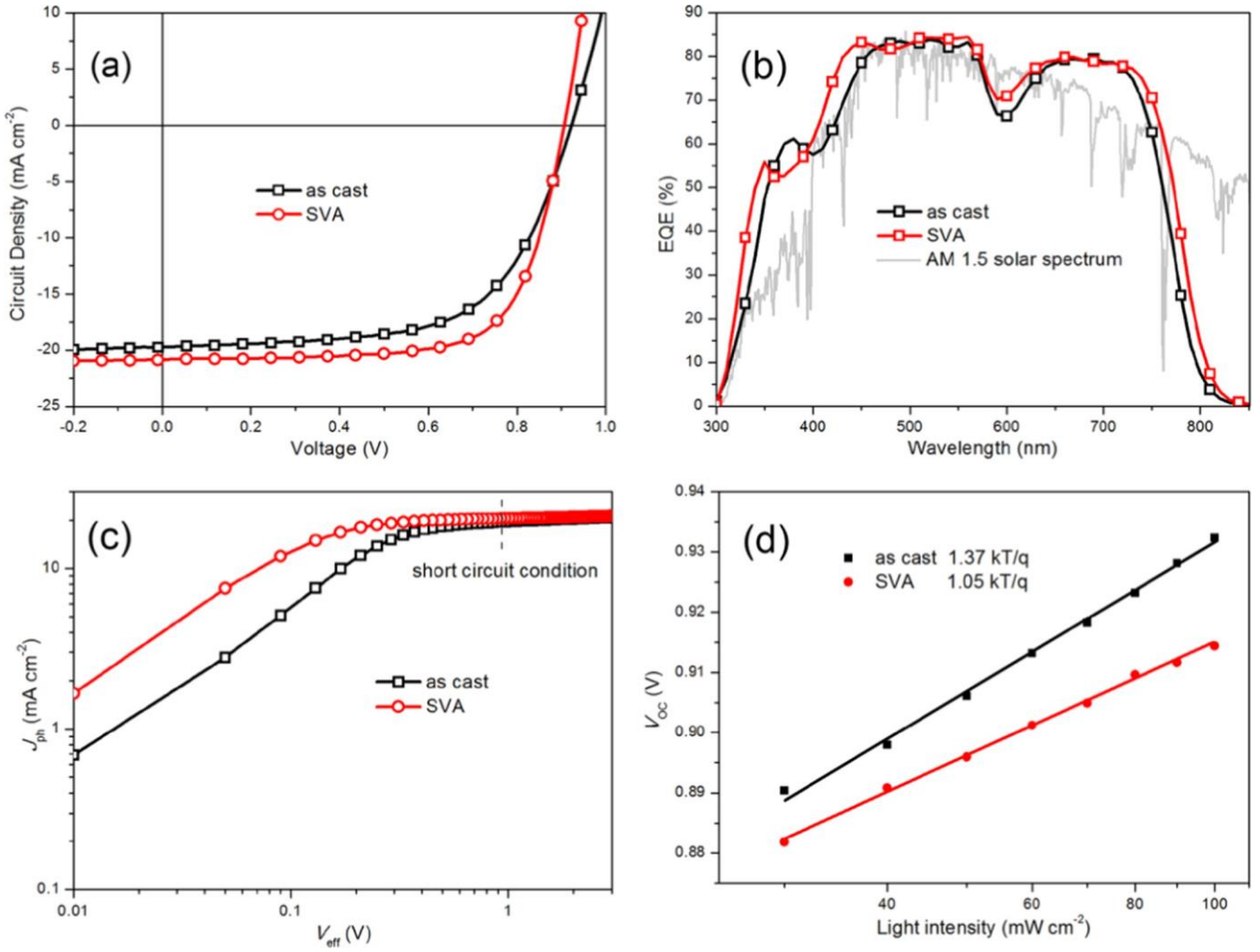

Figure 2. Solar cell parameters for the devices based on PBB-T:ITIC-F (1:1.2, w/w): (a) $J-V$ curves, (b) EQE spectra, (c) J_{ph} versus V_{eff} characteristics, and (d) dependence of V_{oc} on the light intensity.

Table 2. Photovoltaic Performance of the PSCs Based on PBB-T:ITIC-F (1:1.2, w/w) under the Illumination of AM 1.5 G, 100 mw cm^{-2}

devices[a]	V_{OC} (V)	J_{SC} (mA cm^{-2})	FF	PCE$_{max}$ (%)	R_s (Ω cm^2)[c]	R_{sh} (kΩ cm^2)[d]
as cast	0.92 (0.91 ± 0.01)	19.7 (19.3 ± 0.2)	0.62 (0.59 ± 0.02)	11.3 (11.1 ± 0.1)[b]	7.65	0.77
SVA[e]	0.91 (0.91 ± 0.01)	20.9 (20.5 ± 0.3)	0.70 (0.68 ± 0.02)	13.3 (13.2 ± 0.1)[b]	4.63	1.84

[a]The active layer thickness is about 110 nm. [b]Average values with standard deviation were obtained from 20 devices. [c]Calculated from the inverse slope at $V = V_{OC}$ of the $J-V$ curves under illumination. [d]Calculated from the inverse slope at $V = 0$ V of the $J-V$ curves under illumination. [e]Solvent vapor annealing in chlorobenzene atmosphere for 10 min.

voltage.[44] It is observed that J_{ph} increased linearly at low values of V_{eff} and reached saturation (J_{sat}) at high V_{eff} (≥2 V), suggesting that photogenerated excitons are dissociated into free carriers and collected by the electrodes. The charge dissociation probability ($P(E, T)$) can be calculated from J_{ph}/J_{sat}. Under short-circuit conditions, the $P(E, T)$ of the as-cast and SVA devices are 96 and 98% (Figure S8), respectively, indicating that SVA is in favor of efficient exciton dissociation and charge collection.

To investigate the influence of SVA on the charge recombination, the dependence of the V_{OC} on the light intensity (P) is estimated, which can be used to estimate the extent of trap-assisted recombination in the device. In general, the slope of V_{OC} versus ln P is equal to kT/q if bimolecular recombination is dominating. However, if trap-assisted recombination is dominating, the slope is equal to $2kT/q$.[45] Figure 2d shows the semilogarithmic plot of V_{OC} versus P. The as-cast device shows a larger slope of $1.37kT/q$ compared with the SVA device ($1.05kT/q$), indicating that SVA suppresses trap-assisted recombination, which is beneficial for improving the J_{SC} and FF values.

Film Morphology Analysis. To understand the effect of solvent vapor annealing on the film surface morphology, tapping-mode atomic force microscopy (AFM) was employed to map the surfaces (Figure S9) of the PBB-T/ITIC absorber layers without and with SVA. Both films show similarly smooth morphologies with root mean square (RMS) roughness values of 1.09 and 1.17 nm for the as-cast and solvent-annealed blend films, respectively. To investigate the crystallization behavior and molecular packing of PBB-T and the PBB-T/ITIC-F

DOI: 10.1021/acs.chemmater.8b04265
Chem. Mater. 2019, 31, 919−926

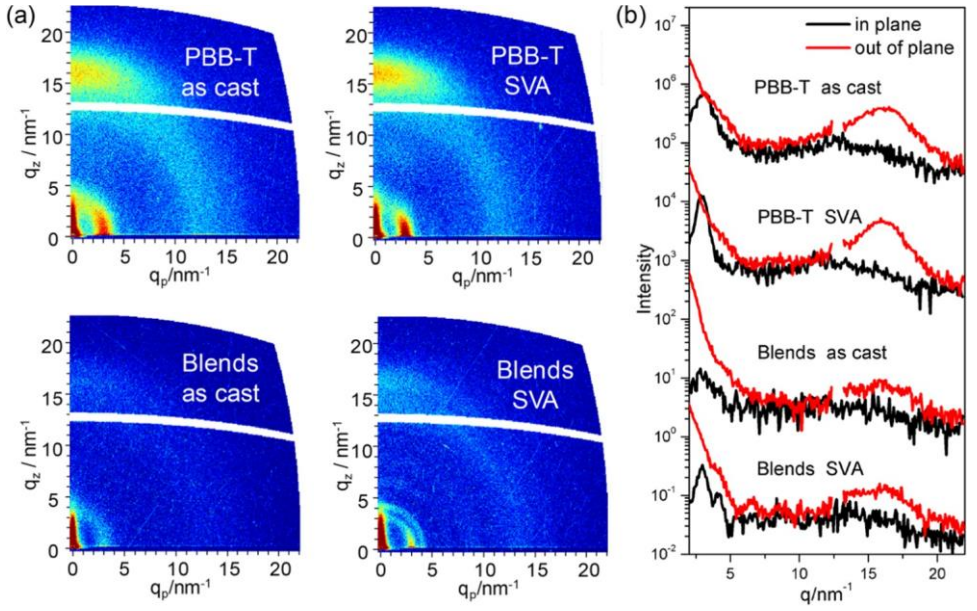

Figure 3. (a) Two-dimensional (2D) GIWAXS patterns and (b) scattering profiles for pristine PBB-T and blend films of PBB-T:ITIC-F. The scattering profiles are shifted vertically for better visibility.

blend, grazing-incidence wide-angle X-ray scattering (GIWAXS) measurements were performed. Thin films of PBB-T and blends of the polymer with ITIC-F (spin coated on silicon substrates) were examined before and after solvent vapor annealing. Figure 3 presents the two-dimensional GIWAXS q-patterns of the pristine polymers and blend films and the corresponding in-plane and out-of-plane line-cut profiles. Generally, an intense diffraction peak at $q = 3$ nm^{-1} in the in-plane direction and a circle-like feature at $q = 16-17$ nm^{-1} in the out-of-plane direction are observed in the PBB-T pristine films, which correspond to an interlamellar distance of approximately 2.1 nm and a $\pi-\pi$ stacking distance of approximately 0.38 nm. This diffraction feature is also indicative of the preferred face-on orientation of the polymer chains.

It is noteworthy that solvent vapor annealing increases the crystallinity and ordering in the pristine film of PBB-T. This is mainly indicated by the significant narrowing along with an increased intensity of the peak at $q = 3$ nm^{-1} in the in-plane direction as can be clearly observed in Figure 3b. By comparing the full width half maximum (FWHM) of the Bragg peak at $q = 3.0$ nm^{-1}, it can be seen that after solvent annealing, the FWHM decreases (from 1.3 to 0.78 nm^{-1}), whereas the peak area increases from 0.70 to 0.92 (Gauss fit). Since the peak area is proportional to the number of molecular planes that participate in crystalline stacking,[46] it can be concluded that the solvent-annealing procedure increases the crystallinity. The peak width reflects the coherence length and indicates that the crystal size and quality (coherence length) are increasing in the q_y direction (e.g., crystallites parallel to the surface) from 4.8 to 8.1 nm, which is in favor of achieving higher mobility. Moreover, the higher degree of order in the solvent vapor-annealed polymer films is supported by the fact that the intensity of the circular extension (random orientation) of the diffraction peak at $q = 3$ nm^{-1} is reduced, suggesting a more defined face-on orientation.

In the blend films of PBB-T and ITIC-F, the features observed in the pristine polymer become much weaker, but are still observable. After the solvent vapor annealing of the PBB-T/ITIC-F blend film, the features again become more intense and defined. In addition, next to the diffraction peak at $q = 3$ nm^{-1}, which is extended to a circle-like pattern (already present in the pristine polymer film), a second distinct circle-like scattering is found at $q = 4.1$ nm^{-1} in the GIWAXS images. This correlates to a lamellar stacking distance of 1.5 nm and originates most likely from ITIC-F phases in the blend films.[47] The presence of scattering features characteristic of stacked molecules of both components, PBB-T as well as ITIC-F, indicates that phase-separated domains are formed as usually observed for bulk heterojunction absorber layers. These domains still have a certain degree of crystallinity, which is further increased after solvent vapor annealing and typically leads to better charge transport properties in the layer. Charge carrier mobilities of PBB-T:ITIC-F blend films were measured by using the space charge limited current (SCLC) method (Figure S10). The hole (μ_h)/electron (μ_e) mobilities were calculated to be $2.70 \times 10^{-5}/9.11 \times 10^{-5}$ cm^2 V^{-1} s^{-1} for the as-cast and $1.93 \times 10^{-4}/1.74 \times 10^{-4}$ cm^2 V^{-1} s^{-1} for the solvent vapor-annealed blend films, which are comparable to the values for other conjugated polymers used in organic photovoltaics.[10,13,15,19,23,30] Solvent vapor annealing improved both the hole and electron mobilities; especially the hole mobility increased by nearly one order of magnitude, and the ratio of μ_h/μ_e is close to 1, which results in a more balanced charge transport. Ordered packing, preferable orientation, and balanced charge transport are assumed to synergistically contribute to the high J_{SC} and FF values of the solar cells.

CONCLUSIONS

In conclusion, we applied the wide-bandgap conjugated polymer PBB-T based on benzobis(thiazole) (BBT) in non-fullerene polymer solar cells. The polymer PBB-T exhibits an optical band gap of 2.10 eV with absorption peaks at 515 and 554 nm, matching well with the strongest region of the solar radiation spectrum. With the PBB-T:ITIC-F blends as the active layer, high power conversion efficiencies of up to 13.3% were obtained with a V_{OC} of 0.91 V, a J_{SC} of 20.9 mA cm^{-2},

DOI: 10.1021/acs.chemmater.8b04265
Chem. Mater. 2019, 31, 919−926

and an FF of 0.70 in non-fullerene PSC devices. Solvent vapor annealing effectively improved the molecular orientation and crystallinity, charge carrier mobilities, and exciton dissociation, which contribute to the amazing J_{SC}, FF, and efficiency. EQE spectra exhibited high quantum efficiency values of over 80% in the wavelength from 430 to 570 nm, indicating effective utilization of the strongest region of the solar radiation, which contributes to achieve these high J_{SC} values. This work has shown that the combination of PBB-T:ITIC-F is an excellent donor−acceptor pair and further device optimization might increase the efficiencies to even higher values. In addition, the benzobis(thiazole) unit is a promising building block for constructing highly efficient polymers for non-fullerene solar cells, especially considering its versatility in modifying the molecular structure. The investigation on the performance of modified BBT-based materials is currently in progress.

EXPERIMENTAL SECTION

Materials and Measurements. All reactions were carried out in an inert atmosphere. PBB-T[37] and ITIC-F[41] were synthesized according to the literature methods. Other reagents were purchased from commercial sources and used directly unless otherwise noted. ^{1}H NMR and ^{13}C NMR spectra were recorded using a Bruker AVANCE-III 600 spectrometer with tetramethylsilane as an internal standard. The molecular weights of the polymers were measured by GPC using 1,2,4-trichlorobenzene (TCB) as the solvent and polystyrene as the standard at 150 °C. Thermogravimetric analysis was performed in an SDT Q600 setup with a heating rate of 10 °C min^{-1} under a nitrogen atmosphere. Cyclic voltammetry was measured on a CHI660D electrochemical workstation in a solution of tetrabutylammonium hexafluorophosphate (Bu_4NPF_6, 0.1 M) in acetonitrile at a scan rate of 100 mV s^{-1}. The three-electrode system was composed of a glass carbon electrode coated with the sample film as the working electrode, a Pt wire as the counter electrode, and a saturated calomel electrode (SCE) as the reference electrode. Potentials were referenced to the ferrocene/ferrocenium (Fc/Fc^+) couple by using ferrocene as the standard. Atomic force microscopy measurements were performed using an Agilent 5400 AFM in tapping mode under ambient conditions. UV−vis absorption spectra were obtained on a Perkin Elmer Lambda 25 spectrophotometer. Photoluminescence (PL) spectra were measured on a Perkin Elmer LS-50 luminescence spectrometer. All film samples were spin coated on quartz glass substrates.

Fabrication of Photovoltaic Devices. Conventional PSC devices were fabricated with the configuration of ITO/PEDOT:PSS/PBB-T:ITIC-F/PDINO/Al. The ITO-coated glass substrates with a nominal sheet resistance of 15 Ω sq^{-1} were cleaned in an ultrasonic bath with detergent, ultrapure water, acetone, and isopropyl alcohol. After a 10 min oxygen plasma treatment, a thin layer of PEDOT:PSS (30 nm) was spin coated onto the ITO anode and then dried at 160 °C for 20 min. The polymer PBB-T and ITIC-F were dissolved in chlorobenzene with a concentration of 7 mg mL^{-1} for PBB-T. The solution was stirred for several hours at 90 °C and spin coated on the PEDOT:PSS layer. The thickness of the active layer was ∼100 nm. Then, a thin layer of PDINO was spin coated onto the active layer at 4000 rpm for 30 s from the methanol solution (1.0 mg/mL). Finally, 100 nm Al layers were successively thermally evaporated onto the active layer at a pressure of 4.0×10^{-4} Pa. The active area of the device in this work was 0.1 cm^2. The current density−voltage ($J-V$) characteristics were recorded with a Keithley 2420 source measure unit under AM 1.5G illumination (100 mW cm^{-2}) from a Newport solar simulator. A standard silicon solar cell was used to calibrate the light intensity. The external quantum efficiencies (EQE) of the PSCs were measured using a certified Newport incident photon conversion efficiency measurement system.

Mobility Measurements. Hole-only or electron-only devices were fabricated using the architectures ITO/PEDOT:PSS/PBB-T:ITIC-F/MoO_3/Al for holes and ITO/ZnO/PBB-T:ITIC-F/PDINO/Al for electrons. The mobility was extracted by fitting the current density−voltage curves using space charge limited current (SCLC), which is described by the equation

$$\frac{2}{} \quad \frac{V^2}{}$$

DOI: 10.1021/acs.chemmater.8b04265
Chem. Mater. 2019, 31, 919−926

$$J = \frac{9\varepsilon_0\varepsilon_r\mu_h V^2}{8d^3}$$

where J is the current, μ_h is the zero-field mobility, and ε_0 and ε_r are the permittivity of free space and relative permittivity of the material, respectively. V is the effective voltage and d is the thickness of the organic layer. The effective voltage can be obtained by subtracting the built-in voltage (V_{bi}) and the voltage drop (V_s) from the substrate's series resistance from the applied voltage (V_{appl}): $V = V_{appl} - V_{bi} - V_s$. The hole and electron mobilities can be calculated from the slope of the $J^{1/2}-V$ curves.

GIWAXS Characterization. For the 2D-GIWAXS characterizations, thin films of the polymer and polymer/ITIC-F blends spin coated on silicon substrates were used. 2D-GIWAXS measurements were performed on an Anton Paar SAXSpoint 2.0 system equipped with a Dectris 2D EIGER R 1M hybrid photon-counting detector with 75 μm^2 pixel size and using Cu Kα radiation at 50 kV and 1 mA, which was point collimated using automated scatterless slits. The incidence angle was set to 0.12° and the exposure time was 10 × 120 s. A spin-coated silver behenate film was used for angular calibration.

ASSOCIATED CONTENT

Supporting Information

The Supporting Information is available free of charge on the ACS Publications website at DOI: 10.1021/acs.chemma- ter.8b04265.

Details of materials and measurements, optical and GIWAXS characterizations, fabrication of PSC devices, synthetic routes of PBB-T and ITIC-F, analytical data, photoluminescence spectra, photovoltaic data, mobi- lities, statistics of PCEs of several devices, AFM height images, and NMR spectra (PDF)

AUTHOR INFORMATION

Corresponding Authors

*E-mail: wensg@qibebt.ac.cn (S.W.).
*E-mail: gregor.trimmel@tugraz.at (G.T.).
*E-mail: yangrq@qibebt.ac.cn (R.Y.).

ORCID

Shuguang Wen: 0000-0001-9181-9019
Thomas Rath: 0000-0002-4837-7726
Yonghai Li: 0000-0002-5748-0258
Xichang Bao: 0000-0001-7325-7550
Gregor Trimmel: 0000-0001-8922-4163
Yong Zhang: 0000-0001-7718-5945
Renqiang Yang: 0000-0001-6794-7416

Notes

The authors declare no competing financial interest.

ACKNOWLEDGMENTS

This work was supported by the Ministry of Science and Technology of China (2016YFE0115000 and 2014CB643501), the National Natural Science Foundation of China (21202181, 51573205, and 51773220), and the Department of Science and Technology of Shandong Province (2015GGX104007 and ZR2017ZB0314). T.R. and G.T. acknowledge financial support by the OEAD S&T Cooperation program (project number CN 01/2016).

DOI: 10.1021/acs.chemmater.8b04265
Chem. Mater. 2019, 31, 919−926

REFERENCES

(1) Service, R. F. Outlook Brightens for Plastic Solar Cells. *Science* 2011, *332*, 293.

(2) Li, Y. Molecular Design of Photovoltaic Materials for Polymer Solar Cells: toward Suitable Electronic Energy Levels and Broad Absorption. *Acc. Chem. Res.* 2012, *45*, 723−733.

(3) Yu, G.; Gao, J.; Hummelen, J. C.; Wudl, F.; Heeger, A. J. Polymer Photovoltaic Cells - Enhanced Efficiencies via a Network of Internal Donor-Acceptor Heterojunctions. *Science* 1995, *270*, 1789−1791.

(4) Lu, L.; Zheng, T.; Wu, Q.; Schneider, A. M.; Zhao, D.; Yu, L. Recent Advances in Bulk Heterojunction Polymer Solar Cells. *Chem. Rev.* 2015, *115*, 12666−12731.

(5) Li, G.; Chang, W.-H.; Yang, Y. Low-Bandgap Conjugated Polymers Enabling Solution-Processable Tandem Solar Cells. *Nat. Rev. Mater.* 2017, *2*, No. 17043.

(6) Li, G.; Zhu, R.; Yang, Y. Polymer Solar Cells. *Nat. Photonics* 2012, *6*, 153−161.

(7) Cheng, Y.-J.; Yang, S.-H.; Hsu, C.-S. Synthesis of Conjugated Polymers for Organic Solar Cell Applications. *Chem. Rev.* 2009, *109*, 5868−5923.

(8) Dominguez, I. F.; Distler, A.; Luer, L. Stability of Organic Solar Cells: the Influence of Nanostructured Carbon Materials. *Adv. Energy Mater.* 2017, *7*, No. 1601320.

(9) Lin, Y.; Wang, J.; Zhang, Z. G.; Bai, H.; Li, Y.; Zhu, D.; Zhan, X. An Electron Acceptor Challenging Fullerenes for Efficient Polymer Solar Cells. *Adv. Mater.* 2015, *27*, 1170−1174.

(10) Bin, H.; Gao, L.; Zhang, Z. G.; Yang, Y.; Zhang, Y.; Zhang, C.; Chen, S.; Xue, L.; Yang, C.; Xiao, M.; Li, Y. 11.4% Efficiency Non-Fullerene Polymer Solar Cells with Trialkylsilyl Substituted 2D-Conjugated Polymer as Donor. *Nat. Commun.* 2016, *7*, No. 13651.

(11) Fan, B.; Ying, L.; Zhu, P.; Pan, F.; Liu, F.; Chen, J.; Huang, F.; Cao, Y. All-Polymer Solar Cells Based on a Conjugated Polymer Containing Siloxane-Functionalized Side Chains with Efficiency over 10%. *Adv. Mater.* 2017, *29*, No. 1703906.

(12) Gao, W.; An, Q. S.; Ming, R. J.; Xie, D. J.; Wu, K. L.; Luo, Z. H.; Zou, Y.; Zhang, F. J.; Yang, C. L. Side Group Engineering of Small Molecular Acceptors for High-Performance Fullerene-Free Polymer Solar Cells: Thiophene Being Superior to Selenophene. *Adv. Funct. Mater.* 2017, *27*, No. 1702194.

(13) Kan, B.; Feng, H.; Wan, X.; Liu, F.; Ke, X.; Wang, Y.; Wang, Y.; Zhang, H.; Li, C.; Hou, J.; Chen, Y. Small-Molecule Acceptor Based on the Heptacyclic Benzodi(cyclopentadithiophene) Unit for Highly Efficient Nonfullerene Organic Solar Cells. *J. Am. Chem. Soc.* 2017, *139*, 4929−4934.

(14) Li, S.; Zhan, L.; Liu, F.; Ren, J.; Shi, M.; Li, C. Z.; Russell, T. P.; Chen, H. An Unfused-Core-Based Nonfullerene Acceptor Enables High-Efficiency Organic Solar Cells with Excellent Morphological Stability at High Temperatures. *Adv. Mater.* 2018, *30*, No. 1705208.

(15) Li, Y.; Lin, J. D.; Che, X.; Qu, Y.; Liu, F.; Liao, L. S.; Forrest, S. R. High Efficiency Near-Infrared and Semitransparent Non-Fullerene Acceptor Organic Photovoltaic Cells. *J. Am. Chem. Soc.* 2017, *139*, 17114−17119.

(16) Zhang, G.; Zhao, J.; Chow, P. C. Y.; Jiang, K.; Zhang, J.; Zhu, Z.; Zhang, J.; Huang, F.; Yan, H. Nonfullerene Acceptor Molecules for Bulk Heterojunction Organic Solar Cells. *Chem. Rev.* 2018, *118*, 3447−3507.

(17) Hwang, Y. J.; Li, H.; Courtright, B. A.; Subramaniyan, S.; Jenekhe, S. A. Nonfullerene Polymer Solar Cells with 8.5% Efficiency Enabled by a New Highly Twisted Electron Acceptor Dimer. *Adv. Mater.* 2016, *28*, 124−131.

(18) Kan, B.; Zhang, J.; Liu, F.; Wan, X.; Li, C.; Ke, X.; Wang, Y.; Feng, H.; Zhang, Y.; Long, G.; Friend, R. H.; Bakulin, A. A.; Chen, Y. Fine-Tuning the Energy Levels of a Nonfullerene Small-Molecule Acceptor to Achieve a High Short-Circuit Current and a Power Conversion Efficiency over 12% in Organic Solar Cells. *Adv. Mater.* 2018, *30*, No. 1704904.

(19) Yao, Z.; Liao, X.; Gao, K.; Lin, F.; Xu, X.; Shi, X.; Zuo, L.; Liu, F.; Chen, Y.; Jen, A. K. Dithienopicenocarbazole-Based Acceptors for Efficient Organic Solar Cells with Optoelectronic Response over 1000 nm and an Extremely Low Energy Loss. *J. Am. Chem. Soc.* 2018, *140*, 2054−2057.

(20) Xu, S. J.; Zhou, Z.; Liu, W.; Zhang, Z.; Liu, F.; Yan, H.; Zhu, X. A Twisted Thieno[3,4-b]thiophene-Based Electron Acceptor Featuring a 14-pi-Electron Indenoindene Core for High-Performance Organic Photovoltaics. *Adv. Mater.* 2017, *29*, No. 1704510.

(21) Yao, H.; Cui, Y.; Yu, R.; Gao, B.; Zhang, H.; Hou, J. Design, Synthesis, and Photovoltaic Characterization of a Small Molecular Acceptor with an Ultra-Narrow Band Gap. *Angew. Chem., Int. Ed.* 2017, *56*, 3045−3049.

(22) Holliday, S.; Ashraf, R. S.; Nielsen, C. B.; Kirkus, M.; Rohr, J. A.; Tan, C. H.; Collado-Fregoso, E.; Knall, A. C.; Durrant, J. R.; Nelson, J.; McCulloch, I. A Rhodanine Flanked Nonfullerene Acceptor for Solution-Processed Organic Photovoltaics. *J. Am. Chem. Soc.* 2015, *137*, 898−904.

(23) Liu, R.; Du, Z.; Wen, S.; Wu, Y.; Zhu, D.; Yang, R. Energy Levels Modulation of Small Molecule Acceptors for Polymer Solar Cells. *Synth. Met.* 2018, *235*, 131−135.

(24) Bin, H.; Zhang, Z. G.; Gao, L.; Chen, S.; Zhong, L.; Xue, L.; Yang, C.; Li, Y. Non-Fullerene Polymer Solar Cells Based on Alkylthio and Fluorine Substituted 2D-Conjugated Polymers Reach 9.5% Efficiency. *J. Am. Chem. Soc.* 2016, *138*, 4657−4664.

(25) Xu, X.; Yu, T.; Bi, Z.; Ma, W.; Li, Y.; Peng, Q. Realizing Over 13% Efficiency in Green-Solvent-Processed Nonfullerene Organic Solar Cells Enabled by 1,3,4-Thiadiazole-Based Wide-Bandgap Copolymers. *Adv. Mater.* 2018, *30*, No. 1703973.

(26) Lin, Y.; Zhao, F.; Wu, Y.; Chen, K.; Xia, Y.; Li, G.; Prasad, S. K.; Zhu, J.; Huo, L.; Bin, H.; Zhang, Z. G.; Guo, X.; Zhang, M.; Sun, Y.; Gao, F.; Wei, Z.; Ma, W.; Wang, C.; Hodgkiss, J.; Bo, Z.; Inganas, O.; Li, Y.; Zhan, X. Mapping Polymer Donors toward High-Efficiency Fullerene Free Organic Solar Cells. *Adv. Mater.* 2017, *29*, No. 1604155.

(27) Yao, H.; Yu, R.; Shin, T. J.; Zhang, H.; Zhang, S.; Jang, B.; Uddin, M. A.; Woo, H. Y.; Hou, J. A Wide Bandgap Polymer with Strong π-π Interaction for Efficient Fullerene-Free Polymer Solar Cells. *Adv. Energy Mater.* 2016, *6*, No. 1600742.

(28) Chen, S.; Liu, Y.; Zhang, L.; Chow, P. C. Y.; Wang, Z.; Zhang, G.; Ma, W.; Yan, H. A Wide-Bandgap Donor Polymer for Highly Efficient Non-Fullerene Organic Solar Cells with a Small Voltage Loss. *J. Am. Chem. Soc.* 2017, *139*, 6298−6301.

(29) Guo, B.; Li, W.; Guo, X.; Meng, X.; Ma, W.; Zhang, M.; Li, Y. High Efficiency Nonfullerene Polymer Solar Cells with Thick Active Layer and Large Area. *Adv. Mater.* 2017, *29*, No. 1702291.

(30) Zhang, S.; Qin, Y.; Zhu, J.; Hou, J. Over 14% Efficiency in Polymer Solar Cells Enabled by a Chlorinated Polymer Donor. *Adv. Mater.* 2018, *30*, No. 1800868.

(31) Zhao, W.; Zhang, S.; Zhang, Y.; Li, S.; Liu, X.; He, C.; Zheng, Z.; Hou, J. Environmentally Friendly Solvent-Processed Organic Solar Cells that are Highly Efficient and Adaptable for the Blade-Coating Method. *Adv. Mater.* 2018, *30*, No. 1704837.

(32) Zhao, W.; Qian, D.; Zhang, S.; Li, S.; Inganas, O.; Gao, F.; Hou, J. Fullerene-Free Polymer Solar Cells with over 11% Efficiency and Excellent Thermal Stability. *Adv. Mater.* 2016, *28*, 4734−4739.

(33) Tam, T. L. D.; Lin, T. T. Tuning Energy Levels and Film Morphology in Benzodithiophene-Thienopyrrolodione Copolymers via Nitrogen Substitutions. *Macromolecules* 2016, *49*, 1648−1654.

(34) Dess,A.; Consiglio, G. B.; Calamante, M.; Reginato, G.; Mordini, A.; Peruzzini, M.; Taddei, M.; Sinicropi, A.; Parisi, M. L.; de Biani, F. F.; Basosi, R.; Mori, R.; Spatola, M.; Bruzzi, M.; Zani, L. Organic Chromophores Based on a Fused Bis-Thiazole Core and their Application in Dye-Sensitized Solar Cells. *Eur. J. Org. Chem.* 2013, 1916−1928.

(35) Ahmed, E.; Subramaniyan, S.; Kim, F. S.; Xin, H.; Jenekhe, S. A. Benzobisthiazole-Based Donor-Acceptor Copolymer Semiconductors for Photovoltaic Cells and Highly Stable Field-Effect Transistors. *Macromolecules* 2011, *44*, 7207−7219.

(36) Ahmed, E.; Kim, F. S.; Xin, H.; Jenekhe, S. A. Benzobisthiazole-Thiophene Copolymer Semiconductors: Synthesis, Enhanced Stabil-

DOI: 10.1021/acs.chemmater.8b04265
Chem. Mater. 2019, 31, 919−926

ity, Field-Effect Transistors, and Efficient Solar Cells. *Macromolecules* 2009, *42*, 8615−8618.
(37) Bhuwalka, A.; Ewan, M. D.; Elshobaki, M.; Mike, J. F.; Tlach, B.; Chaudhary, S.; Jeffries-El, M. Synthesis and Photovoltaic Properties of 2,6-Bis(2-thienyl) Benzobisazole and 4,8-Bis(thienyl)-benzo[1,2-b:4,5-b′]dithiophene Copolymers. *J. Polym. Sci., Part A: Polym. Chem.* 2016, *54*, 316−324.
(38) Osaka, I.; Takimiya, K.; McCullough, R. D. Benzobisthiazole-Based Semiconducting Copolymers Showing Excellent Environmental Stability in High-Humidity Air. *Adv. Mater.* 2010, *22*, 4993−4997.
(39) Al-Naamani, E.; Gopal, A.; Ide, M.; Osaka, I.; Saeki, A. Exploring Alkyl Chains in Benzobisthiazole-Naphthobisthiadiazole Polymers: Impact on Solar-Cell Performance, Crystalline Structures, and Optoelectronics. *ACS Appl. Mater. Interfaces* 2017, *9*, 37702−37711.
(40) Li, Y.; Wu, Y.; Ong, B. S. Polyindolo[3,2-*b*]carbazoles: A New Class of p-Channel Semiconductor Polymers for Organic Thin-Film Transistors. *Macromolecules* 2006, *39*, 6521−6527.
(41) Yang, F.; Li, C.; Lai, W.; Zhang, A.; Huang, H.; Li, W. Halogenated Conjugated Molecules for Ambipolar Field-Effect Transistors and Non-Fullerene Organic Solar Cells. *Mater. Chem. Front.* 2017, *1*, 1389−1395.
(42) Yao, H.; Qian, D.; Zhang, H.; Qin, Y.; Xu, B.; Cui, Y.; Yu, R.; Gao, F.; Hou, J. Critical Role of Molecular Electrostatic Potential on Charge Generation in Organic Solar Cells. *Chin. J. Chem.* 2018, *36*, 491−494.
(43) Zhang, Z.-G.; Qi, B.; Jin, Z.; Chi, D.; Qi, Z.; Li, Y.; Wang, J. Perylene Diimides: A Thickness-Insensitive Cathode Interlayer for High Performance Polymer Solar Cells. *Energy Environ. Sci.* 2014, *7*, 1966−1973.
(44) Wu, J.-L.; Chen, F.-C.; Hsiao, Y.-S.; Chien, F.-C.; Chen, P.; Kuo, C.-H.; Huang, M. H.; Hsu, C.-S. Surface Plasmonic Effects of Metallic Nanoparticles on the Performance of Polymer Bulk Heterojunction Solar Cells. *ACS Nano* 2011, *5*, 959−967.
(45) Koster, L. J. A.; Mihailetchi, V. D.; Ramaker, R.; Blom, P. W. M. Light Intensity Dependence of Open-Circuit Voltage of Polymer:-Fullerene Solar Cells. *Appl. Phys. Lett.* 2005, *86*, No. 123509.
(46) Sung, M. J.; Luzio, A.; Park, W.-T.; Kim, R.; Gann, E.; Maddalena, F.; Pace, G.; Xu, Y.; Natali, D.; de Falco, C.; Dang, L.; McNeill, C. R.; Caironi, M.; Noh, Y.-Y.; Kim, Y.-H. High-Mobility Naphthalene Diimide and Selenophene-Vinylene-Selenophene-Based Conjugated Polymer: n-Channel Organic Field-Effect Transistors and Structure−Property Relationship. *Adv. Funct. Mater.* 2016, *26*, 4984−4997.
(47) Yuan, J.; Ford, M.; Ding, G.; Dong, H.; Wang, M.; Han, L.; Li, Y.; Bazan, G. C.; Ma, W. Narrow Bandgap Conjugated Polymers Based on a High-Mobility Polymer Template for Visibly Transparent Photovoltaic Devices. *J. Mater. Chem. A* 2016, *4*, 17333−17343.

DOI: 10.1021/acs.chemmater.8b04265
Chem. Mater. 2019, 31, 919−926